Journal of CO_2 Utilization 30 (2019) 214–221

Contents lists available at ScienceDirect

Journal of CO_2 Utilization

journal homepage: www.elsevier.com/locate/jcou

Enhanced selectivity of carbonaceous products from electrochemical reduction of CO_2 in aqueous media

Hang Xiang[a], Shahid Rasul[a,b], Keith Scott[a], Jose Portoles[a], Peter Cumpson[a], Eileen H. Yu[a,*]

[a] School of Engineering, Newcastle University, Newcastle Upon Tyne, United Kingdom
[b] Faculty of Engineering and Environment, Northumbria University, Newcastle Upon Tyne, United Kingdom

ARTICLE INFO

Keywords:
CO_2electrochemical reduction
Aqueous electrolyte
Gas diffusion electrode
Selectivity
Electrochemical catalysis

ABSTRACT

This study highlights the importance of CO_2 supply method and impact of electrolyte alkalinity in aqueous electrochemical CO_2 reduction using Cu_xO catalyst. Two different CO_2 supply methods using a two-chamber (2C) cell with CO_2 purging into catholyte and a CO_2 gas diffusion electrode (GDE) cell were compared. Faradaic efficiency (FE) of carbonaceous products in GDE cell was more than 3-folds higher than the 2C cell due to improved CO_2 mass transfer. From the investigation of alkaline catholyte in GDE cell, the higher catholyte alkalinity led to higher current density and higher FE of carbonaceous products with a better selectivity of C_2 (ethanol and ethylene). The reason lies in the OH groups around catalyst surface which improve the reaction kinetics and moreover stabilize the catalyst surface oxygen during the reduction process. With the potential of -1.17 V (RHE) in 2.0 M KOH, C_2 FE of 40% and current density of -234 mA cm^{-2} were achieved. The production rate of ethylene and ethanol was respectively 0.105 mg min^{-1} and 0.035 mg min^{-1} on 2 cm^2 electrode with CO_2 flow rate 15 ml min^{-1}, which are promising for further development and scale-up.

1. Introduction

The increasing demand for energy and challenges from environmental issues and climate change has led to numerous researches on sustainability and carbon recycling. CO_2 concentration in the atmosphere has reached 427 ppm causing environmental concerns and climate change [1]. Increasing production of renewable energy results in demands on energy storage materials and devices. Effectively utilising and directly converting carbon dioxide (CO_2) into fuels as energy storage media and other valuable chemicals could provide a solution. Among the approaches of CO_2 conversion, electrochemical CO_2 reduction reaction (eCO_2RR) attracted large interests as it only consumes water and electricity as the inputs to build hydrocarbons and oxygenates (i.e., alcohols and carboxylic acids) and to release pure O_2 as a by-product on the anodic side. However, hydrogen evolution reaction (HER) shares similar reaction potential (0.0 V vs. RHE) with eCO_2RR and takes place simultaneously. Due to the big energy barrier of CO_2 activation [2], H_2 is theoretically much easier to be produced than carbonaceous products under aqueous eCO_2RR conditions [3,4].

The rate-determining steps for eCO_2RR and HER in the competitive charge transfer are both one-electron reversible process as illustrated in Equation (1) and Equation (2 or 3) respectively [2–4].

$$eCO2\,RR:\ CO_2(aq) + e^- \leftrightarrow CO_2^-(ads) \quad (1)$$

$$HER:\ Acidic:\ H^+ + e^- \leftrightarrow H(ads) \quad (2)$$

$$Neutral/Alkaline:\ H_2O + e^- \leftrightarrow OH^- + H(ads) \quad (3)$$

The reaction rate of the one-electron reversible electrode process is generally defined as Equation (4) [5].

$$R = \frac{j}{nF} = \frac{j_0\left[\frac{C_O(0,t)}{C_O^*}e^{-\alpha f\eta} - \frac{C_R(0,t)}{C_R^*}e^{(1-\alpha)f\eta}\right]}{nF} \quad (4)$$

Where: *j:* local current density (A m^{-2})
n: number of electron transfer, here it is 1
F: faradaic constant (96,485 C mol^{-1})
j_0*:* exchange current density (A m^{-2})
$C_O(0,t)/C_R(0,t)$*:* the surface concentration of oxidant/reduced product at time t
C_O^*/C_R^**:* the bulk concentration of oxidant/reduced product
α: transfer coefficient (= 0~1)
f: a constant (=F/RT)
η: overpotential (V)

The initial rate of either eCO_2RR or HER accords with Equation (4) which is mainly co-determined by the exchange current density j_0, the surface concentration of reactant, and overpotential. The j_0 is primarily

* Corresponding author.
E-mail address: eileen.yu@ncl.ac.uk (E.H. Yu).

https://doi.org/10.1016/j.jcou.2019.02.007
Received 6 December 2018; Received in revised form 11 February 2019; Accepted 12 February 2019
Available online 22 February 2019

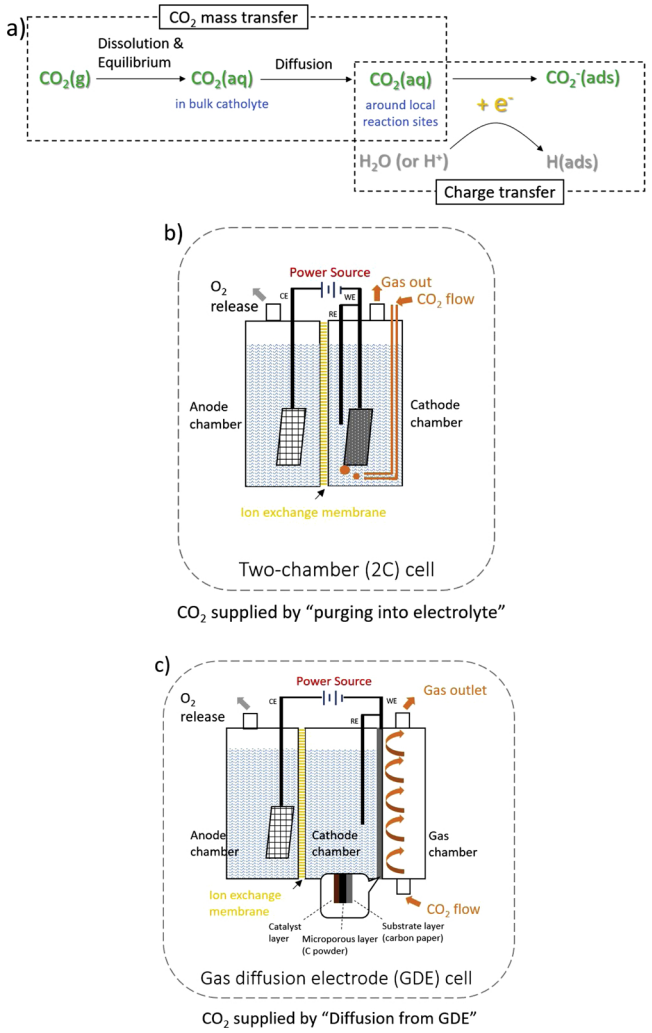

Fig. 1. a) Mass transfer and charge transfer in aqueous eCO_2RR system. Schematic diagrams of aqueous eCO_2RR system using b) 2C cell and c) GDE cell.

related to the adsorption energy of the active species (CO_2^-(ads) and H (ads)) on the electrode material [6]. A suitable catalyst [7] can change the adsorption energy to those species, intending to control the selectivity between carbonaceous products and H_2. In the aqueous eCO_2RR system, the inherent competitive advantage for HER is mass transfer, in another word, the surface concentration of H_2O (or H^+) is always sufficient. However, the mass transfer of heterogeneous CO_2 gas is a more complicated process as illustrated in Fig. 1a.

Majority of publications [8,9] applied a traditional two-chamber (2C) cell where the reactant CO_2 gas was supplied by "purging into electrolyte", as shown in Fig. 1b. CO_2 mass transport is determined by CO_2 solubility. Different approaches have been carried out to increase CO_2 solubility in the electrolytes, such as altering the reaction environment with high pressure [10–12] and low temperature [13], and using alcoholic base [14,15] or ionic liquid [16] as the electrolyte. However, comparing with the ambient pressure, room temperature and aqueous electrolytes, those approaches carry their own set of cost and sustainability issues.

The use of a gas diffusion electrode (GDE) changes the CO_2 supply way from "purging into electrolyte" to "diffusion from GDE" as shown in Fig. 1c, which can directly feed CO_2 gas flow to the reaction interface which has been used by fuel cells for a long time [17]. An increasing number of GDE-based studies in aqueous eCO_2RR were published in recent years, commonly achieving a remarkable current density (*j*) and reasonable faradaic efficiency (FE) towards C-products at ambient temperature and pressure, as summarised in Table 1. In the aqueous system with 2C cells, satisfying FE (> 50%) of carbonaceous products have also been reported but the current densities were averagely low (< 10 mA cm^{-2} at moderate potentials around −1.0 V (vs. RHE) [18]) which is about 10-folds less than GDE cells. The application of GDE should be a reliable approach to transition this bench-scale research to industry. For the further optimisation, the real effect of GDE on eCO_2RR and the factors for the high current density achieved in GDE-related studies still need to be explicit.

J. Albo et al. [25] compared the GDE performances with Cu_2O catalyst when CO_2 supplied as gas and when CO_2 supplied in saturated aqueous catholyte. The direct CO_2 gas feeding showed ˜ 3 mA cm^{-2} higher current density and ˜ 9% FE increase in methanol production. However, the reactor dimensions, electrolytes, membrane, applied potential, supply rate of reactants, etc. all have impacts on eCO_2RR performances, an univariate comparison is needed to examine the effect of CO_2 supply method on eCO_2RR. In this work, a 2C cell and a GDE cell were designed in the same dimension and fabricated by 3D printing. Their eCO_2RR performances were compared using the same Cu_xO catalyst, $KHCO_3$ catholyte with various concentrations at a wide range of potentials. The big difference of product distribution disclosed the crucial role of CO_2 mass transfer in the selectivity of carbonaceous products. Compared to the 2C cell, GDE cell with efficient CO_2 mass transfer showed more than 3-folds improvement of FE for carbonaceous products. eCO_2RR performances in GDE cell with $KHCO_3$ and KOH with various concentrations were also investigated.

2. Experimental

2.1. Cell fabrication and set up

The CO_2 supply methods of "purging into electrolyte" and "diffusion

Table 1
Summary of eCO_2RR performance with GDE working electrode from literature.

Cathode	Anode	Electrolyte	Cell voltage/cathode potential (V)	*j* (mA cm^{-2})	FE for main products
Sn-GDE [19]	Pt/C coated membrane pressed GDE	0.1 M $KHCO_3$ (C) 1 M KOH (A)	Cell: -2.75 V	−26	65% Formate
Ag-GDE [20]	Pt/C-GDE	1 M KCl	Cell: -3 V	−90	92% CO
Ag-GDE [21]	Pt/C-GDE	1 M CsOH	Cathode: -1.62 V (vs. Ag/AgCl)	−80	89.8% CO
Cu_xO-GDE [22]	IrO_2-GDE	1 M KOH	Cathode: -0.8 V (vs. RHE)	−400	> 50% C_2
N-doped graphene quantum dots-GDE [23]	IrO_2-GDE	1 M KOH	−1.0 V (vs. RHE)	−240	60% C_2 5% C_3
Pb-GDE [24]	PtRu-GDE	0.5 M K_2SO_4 + 0.5 M H_2SO_4 (C) 1 M KOH (A)	−2 V (vs. SHE)	−330	90% Formate

C: catholyte; A: anolyte.

from GDE" were carried out by two different electrochemical cells respectively: a 2C cell and a GDE cell were designed with the same dimension of the cathodic and anodic chambers, and fabricated by 3D printer (Form 2, Formlabs) using the photoreactive resin (Form 2 Clear Resin, Formlabs). Cell parts were screwed together using metal bolts. The cathodic and anodic chambers were separated by a cation exchange membrane (CEM) (F-950, Fumapem). The cathode used in both cells was Cu_xO painted GDE with the geometric surface area 2 cm^2 and the anode was Platinum plated Titanium mesh with a dimension of 4 cm^2. The schematics of the two cells are as described in Fig. 1b and c. Figure S1 shows the 3D drawings of the two cells set-up, with the design information given below in the Supplementary Data.

2.2. Catalyst synthesis and working electrode preparation

Cu_xO catalyst was synthesized using the hydrothermal method by reduction of Cu acetate (Sigma-Aldrich, 98%) in the solvent of water and ethanol (Sigma-Aldrich, > 99.8%) mixture reported previously [26]. The volume ratio of water and ethanol was controlled as 1:7, i.e., 10 ml water and 70 ml ethanol. The catalyst was dried at 60 °C in an oven (Oven-30S, SciQuip) in air for 8 h.

15 mg catalyst (Cu_xO) was weighed and dispersed in 200 µl isopropanol and 33 µl Nafion suspension (Sigma-Aldrich, 5 wt.%) to prepare the catalyst ink. The ink was sonicated for 20 min before painting onto the surface of carbon paper with gas diffusion layer (GDL) (H2315 I2 C6, Freudenberg). Drying (45 °C, 1~3 min) was applied between each layer. Painting and drying were repeated until the desired Cu_xO catalyst loading of 4~5 mg cm^{-2} was achieved.

2.3. eCO_2RR electrochemical analysis

All the electrochemical reactions and measurements were carried out at ambient temperature and pressure using a potentiostat (Metrohm Autolab PGSTAT128 N). The flow rate of CO_2 (BOC 99.99%) was controlled at 15 ml min^{-1} by a flow meter (Cole-Parmer TMR1-010462). 5 M KOH solution was employed as the anolyte in all the tests. $KHCO_3$ (Alfa Aesar, 99%) and KOH (Emsure®, 85%) solution with different concentrations of 0.1, 0.5, 1.0, and 2.0 M (only in KOH) were used as the catholyte, and the comparison was carried out. Ag/AgCl (RE-5B, BASI, 3 M NaCl, 0.197 V vs. SHE) was used as the reference electrode, and a luggin capillary was applied to prevent it from being damaged in alkaline electrolyte. The applied potentials (vs. Ag/AgCl) in the three-electrode system were all converted to the reversible hydrogen electrode (RHE), thus the potentials stated in this study are referred to RHE unless otherwise stated.

In the 2C cell, CO_2 was purged into catholyte 1 h before electrochemical tests.

In the GDE cell, a peristaltic pump (120U/DM2, Watson Marlow) was used to supply fresh catholyte to maintain the local pH and to remove liquid product for reaction equilibrium. The flow rate was controlled at 0.25 ml min^{-1} under the applied potential −0.17~-0.77 V and at 0.5 ml min^{-1} under the applied potential −0.77~-1.17 V.

Electrochemical characterisations were made by cyclic voltammetry (CV) and electrochemical impedance spectroscopy (EIS). CV was carried out three cycles between 1.4 to −1.0 V with the scan rate 50 mV s^{-1} to initially explore the cathode electrochemical behaviour. The FRA32 M module on the Autolab potentiostat was operated for EIS measurement, which was recorded with an ac-amplitude of 10 mV over the frequency range from 10k Hz to 0.1 Hz either at open circuit voltage (OCV) or at −0.77 V cathodic potential. The impedance spectra were analysed and fitted using NOVA 2.0 software.

eCO_2RR was carried out by chronoamperometry (CA) recording the current at a particular applied potential for 30 min. The current density (j) was calculated based on the geometric surface area 2 cm^2 of the working electrode.

2.4. Product analysis

A gas chromatography (Shimazu Tracera GC-2010) equipped with Barrier Discharge Ionization (BID) detector was used to analyse gas products and alcoholic liquid products. The ShinCarbon ST micro-packed column 80/100 (Restek) was used to quantitatively analyse permanent gases and light hydrocarbons, while the Zebron ZB-WAXplus capillary column (Phenomenex) was used for alcoholic liquids. An ion chromatography (Eco IC, Metrohm) equipped with the "METROHM 6.1005.200″ column was used for quantifying volatile fatty acids (VFA) including formic acid. The faradaic efficiency (FE) for each product was calculated based on Faraday's law (5)[3], where z is the number of electrons transferred for per mole of reactant (e.g., z = 2 for reduction of CO_2 to CO), n is mass of the product from the electrode in moles, F is Faraday's constant (96,500 C mol^{-1}), Q represents the total charge passed.

$$FE = \frac{z\,n\,F}{Q} \tag{5}$$

2.5. Material characterisation of Cu_xO catalyst

X-ray diffraction (XRD) spectrum which showing the crystal structure of the catalyst were obtained by a Philips X-ray diffractometer PW 1730 diffractometer equipped with a Cu X-ray tube (Cu–Kα; λ = 0.154 nm) operated at 40 kV and 40 mA. To determine the elemental compositions and valence states of the electrode surface (~10 nm depth), X-ray photoelectron spectroscopy (XPS) was performed on a Kratos Axis Nova XPS spectrometer using a K-Alpha line X-Ray source (225 W) over an area of approximately 300 × 700 µm. Microstructural characterisation of the catalyst was performed by scanning electron microscopy (SEM, Hitachi SU-70) coupled with an energy dispersive X-ray detector (EDX, Bruker Quantax 400).

3. Results and discussion

3.1. Effect of CO_2 supply method

The two CO_2 supply methods of "purging into electrolyte" and "diffusion from GDE" implemented by 2C cell and GDE cell respectively, were compared through eCO_2RR using the same Cu_xO-painted GDE as the cathode and same $KHCO_3$ catholyte. The catalyst morphology before and after 3 h eCO_2RR in 1.0 M $KHCO_3$ was analysed by SEM and EDX as shown in Figure S2. The fresh catalyst consisted of spherical particles (100 ~ 1000 nm) which became finer after reaction. The EDX analysis (Figure S2) indicated that Cu_xO catalyst was reduced during eCO_2RR since the atomic ratio of copper to oxygen (Cu/O) was increased from 2.81 (before reaction) to 8.13 (after reaction). Since the substance composition and morphology of Cu_xO catalyst changed over the eCO_2RR duration, fresh Cu_xO catalyst was used in each eCO_2RR, with CV measurements in N_2 and CO_2 atmosphere respectively at the beginning. CV results which preliminarily evaluated the reaction behaviour are shown in Figure S3. After CV, eCO_2RRs were carried out by CA at specific fixed potentials (30 min for each potential), the raw data of CAs are given in Figure S4. The normalized FEs for carbonaceous products and H_2, and the average current density of eCO_2RRs in the 2C and GDE cell were calculated and are shown in Table S1. FE sum of all the carbonaceous products and current density (j) taken from Table S1 are presented in Fig. 2.

It can be observed from the comparison between Fig. 2a and b that:

Within the potential range from −0.17 to −1.17 V, the GDE cell produced carbonaceous products with higher FE than the 2C cell. Although the current densities of the two cells were similar at the same catholyte and potential, the current in the 2C cell was mostly associated with HER. Only a small amount of formate and CO were produced when potentials were more negative than −0.37 V in the 2C cell, whereas CO

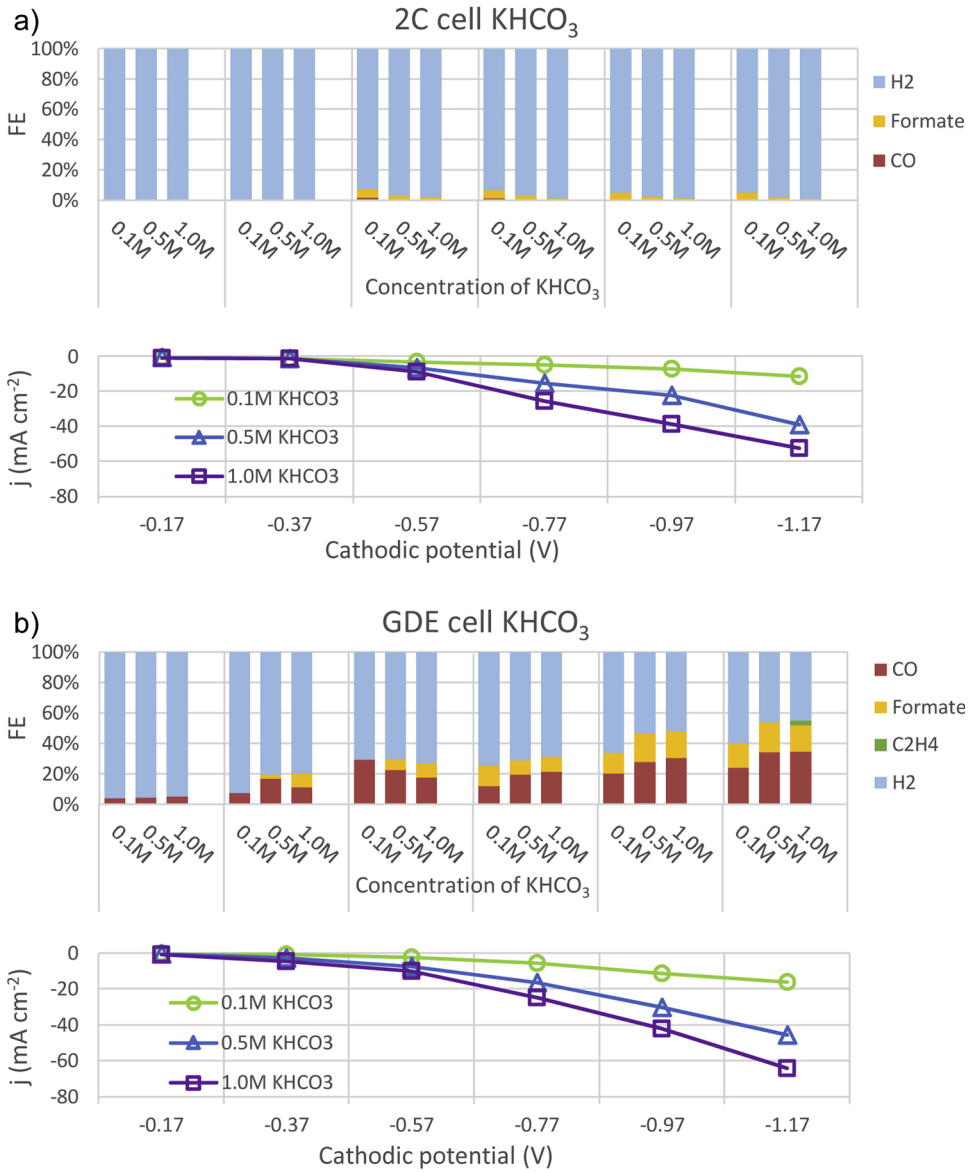

Fig. 2. eCO_2RRs catalysed by Cu_xO at a wide range of applied potentials in a) 2C cell with different concentrations of $KHCO_3$ and b) GDE cell with different concentrations of $KHCO_3$.

was observed from −0.17 V in all $KHCO_3$ electrolytes from GDE cell. The FE of carbonaceous products in GDE cell increased with more negative potential, 5% at −0.17 V to 54% at −1.17 V.

The relationship between total FE of carbonaceous products and $KHCO_3$ catholyte concentration in 2C cell and GDE cell were opposite. In the 2C cell, FE of carbonaceous products decreased with an increase in $KHCO_3$ concentration (a similar result was reported by Hori [27]). However, the GDE cell showed the carbonaceous FE increased with the increasing $KHCO_3$ concentration.

This can be caused by different reaction species from different CO_2 supply method. In the 2C cell, it has been widely accepted that the real reactant in the eCO_2RR system is the dissolved CO_2 (generally written as CO_2 (aq) or H_2CO_3*), rather than ionic HCO_3^- and CO_3 [2–27,1–29]. Although H_2CO_3* concentration increased from higher CO_2 solubility in higher concentration of $KHCO_3$, the CO_2 reduction was determined by the ratio of H_2CO_3*/Total carbonate, which is higher in lower concentrations of $KHCO_3$ according to Heng et al.29] leading to higher selectivity in 0.1 M $KHCO_3$ than in 1.0 M $KHCO_3$.

In aqueous medium, the process of CO_2 mass transfer is composed of two major steps: Step 1. CO_2 gas dissolution and equilibrium to produce the reactant CO_2(aq), Step 2. CO_2(aq) diffusion from bulk catholyte to local reaction sites. The rate of each step and the corresponding influence factors are summarized in Table S2. A brief review related to CO_2 mass transfer process given below Table S2 indicates that $KHCO_3$ with higher concentration can balance slightly more CO_2(aq) in the bulk electrolyte [29] in Step 1, but constrains CO_2(aq) diffusion [30] in Step 2. Moreover, under reduction potential, the K^+ of catholyte would be adsorbed around the double layer that further hinders CO_2(aq) diffusion [31], in favour of hydrogen evolution.

In the GDE cell, the reactant was more likely activated CO_2 species, CO_2*, which the adsorption mechanism as shown in Equation (6) where gaseous CO_2 or CO_2* can be directly reacting at the catalyst interface. The gas adsorption mechanism in GDE was also reported in oxygen reduction reaction (ORR) related studies [32]. With this mass transfer mechanism in GDE cell, sufficient CO_2 reactant could be provided around reaction sites, which develops the competitiveness of eCO_2RR against HER, reflected in a significantly enhanced carbonaceous selectivity than 2C cell.

$$CO_2(g) \xrightarrow{e^-} CO_2^-(ads) \quad (6)$$

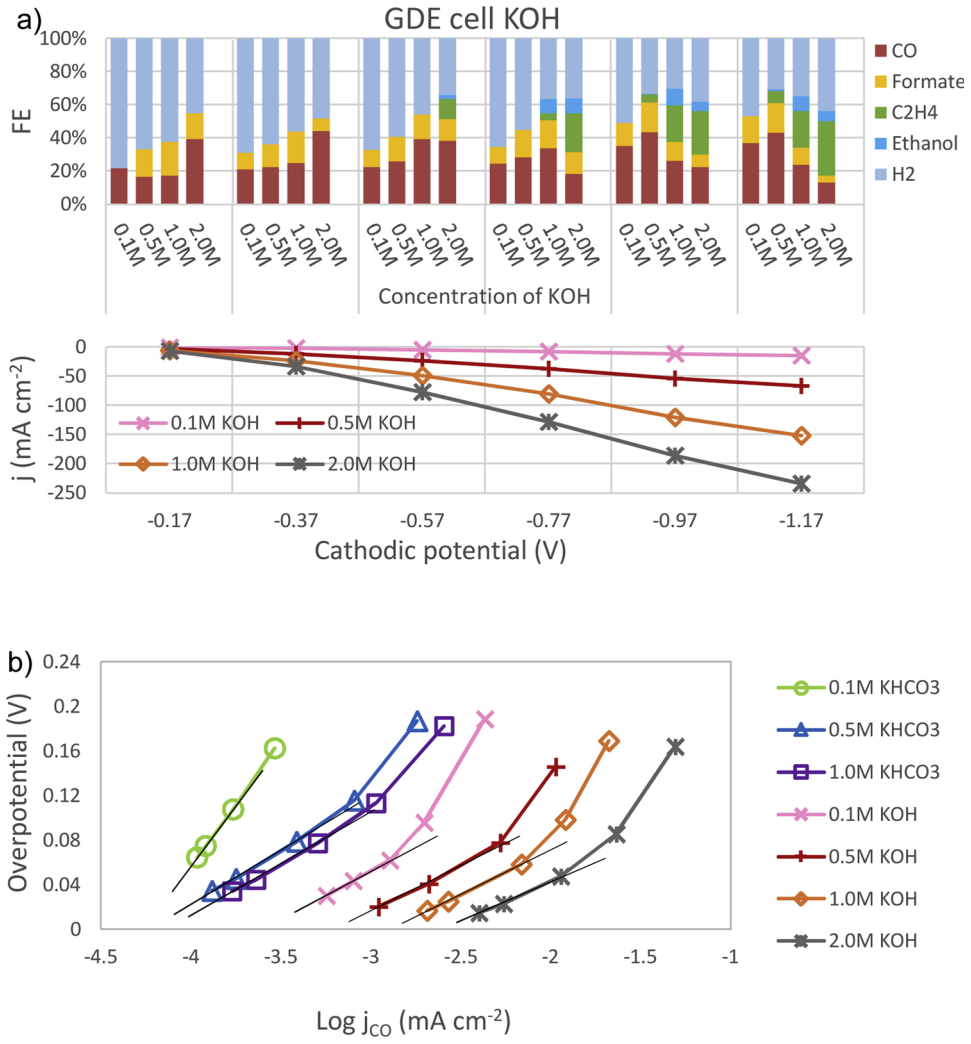

Fig. 3. a) eCO_2RRs catalysed by Cu_xO at a wide range of applied potentials in GDE cell with different concentrations of KOH. b) Tafel plots of the partial current density of CO_2 reduced to CO versus overpotential for CO formation in GDE cell with different catholytes.

In GDE cell, FE of carbonaceous products and current density both increased with the $KHCO_3$ concentration which was probably related to the alkalinity of catholyte. KOH with different concentrations were applied to further study the effect of alkaline catholyte in GDE cell, shown below (Fig. 3a).

3.2. Effect of alkaline catholyte in GDE cell

Fig. 3a shows the eCO_2RR results in GDE cell by applying different concentrations of KOH as the catholyte, Cu_xO was the catalyst. Tafel plots of CO production from eCO_2RR are displayed in Fig. 3b to assess the mechanistic pathway of eCO_2RR in GDE cell with different catholyte since CO was the common product for all the situations and the easiest to be generated at low overpotential. The Tafel slopes show the relationship of IR-corrected overpotential, to eliminate the effect from resistance of the solution, and the log of the partial current density using the actual electrode surface area 108.6 cm^2, which was determined by measuring the double layer capacitance in 0.1 M $HClO_4$ [33] (Figure S5 and Table S3).

Table 2 shows the Tafel parameters of different catholytes in GDE cell obtained from Fig. 3b. With the increasing catholyte pH, the Tafel slope decreased, and the exchange current density $j_0(eCO_2RR)$ for CO production increased, indicating faster kinetics and higher activity of eCO_2RR with more alkaline catholyte. Apart from 0.1 M $KHCO_3$ with lowest $[OH^-]$, the difference between other Tafel slope values were small, decreased from 95 mV dec^{-1} in 0.5 M $KHCO_3$ to 74 mV dec^{-1} in 2.0 M KOH. This suggests the same mechanism for CO_2 reduction to CO despite different $[OH^-]$ in the catholyte.

Table 2
Tafel parameters obtained from the Tafel plots (Fig. 3b), b represents the Tafel slope for the lower overpotential region.

	$KHCO_3$			KOH			
	0.1 M	0.5 M	1.0 M	0.1 M	0.5 M	1.0 M	2.0 M
pH	8.55	9.04	9.67	13.02	13.56	13.96	14.30
b /mV dec^{-1}	213	95	92	90	86	81	74
j_0 /mA cm^{-2}	5.41 $\times10^{-5}$	5.76 $\times10^{-5}$	7.30 $\times10^{-5}$	2.61 $\times10^{-4}$	5.77 $\times10^{-4}$	1.30 $\times10^{-3}$	2.60 $\times10^{-3}$

Comparing eCO_2RR in GDE cell with $KHCO_3$ catholyte (Fig. 2b) and KOH catholyte (Fig. 3a), the selectivity of the carbonaceous products is greater with KOH solution than with $KHCO_3$ solutions shown by higher FE in KOH at the same potentials. Also in both KOH and $KHCO_3$ electrolytes, the carbonaceous FE was enhanced with increasing electrolyte concentrations. 1.0 and 2.0 M KOH at −0.17 V had similar FE of carbonaceous products to $KHCO_3$ at −1.17 V. This 1 V shift suggests lower energy required in catholyte with higher alkalinity.

C_2 products (ethylene and ethanol) were notably produced in KOH catholyte with the concentration higher than 0.5 M. At −1.17 V, the C_2

FE reached almost 40% in 2.0 M KOH. Within the potential range in this study, C_2 selectivity was increased with more negative potentials and higher KOH concentration. Although the highest FE for C_2 was obtained in 2.0 M KOH, the differences between 1.0 and 2.0 M were insignificant indicating the applied potential related to the energy level of the reaction interface at higher pH more critical.

The current density (j) increased with increasing the overpotential and catholyte concentration. Under the same potential, the current density of KOH was much higher than $KHCO_3$ with the same concentration. EIS measurement with the CO_2 atmosphere was used to survey the effect of KOH concentration on resistances. The results displayed in Figure S7 and Table S4 indicate that KOH with higher concentration has smaller resistances of solution and charge transfer. The charge transfer resistance decreased with [OH^-], corresponding to the increasing exchange current density j_0 shown in Table 2. -234 mA cm^{-2} current density was achieved at -1.17 V in 2.0 M KOH, with 40% FE of C_2. The production rate of ethylene and ethanol was respectively 0.105 mg min^{-1} and 0.035 mg min^{-1} on 2 cm^2 electrode with CO_2 flow rate 15 ml min^{-1}, implying the industrialisation potential for C_2 production.

The high alkalinity catholyte showing improved eCO_2RR kinetics and C_2 selectivity could be due to the adsorbed OH on catalyst surface. Zhang et al. [34] compared eCO_2RRs on three different local oxygen-induced surfaces: 1. fully oxidized Cu_2O surface, 2. partially oxidized $Cu(110)-(2\times1)O$ surface, 3. presence of OH spectators. The existence of OH groups as spectators on Cu˚ surface could flip the selectivity between CH_4 and CH_3OH, playing the similar role with the oxidized Cu surface. It has been widely accepted that oxide-derived electrocatalysts applied in eCO_2RR can reduce the energy barrier of CO_2 activation through enhancing the adsorption strength[35] and stability of the active species CO* on reaction sites [3,36,37]. The CO* dimerization is the rate determining step of C_2 products formation [38–42], which occurs at high local pH($\geq$12) [43], and easier to take place on an oxygen-induced Cu surface than bare metallic Cu [44,45].

The use of oxide-derived Cu as the catalyst for CO_2 reduction has been recognized for the purpose of C_2 production in some studies [22,37,44,46,47]. However, J. Albo et al. [48–50] used Cu_2O with 0.5 M $KHCO_3$ catholyte in a two-chamber cell and found methanol to be the major product, which was not detected in this work. Analyzing the methanol absence in this study compared to their work is hard as different type of Cu oxide catalyst applied. Also, the results above indicate, even with the same Cu_xO catalyst, the distribution of carbonaceous products varied by CO_2 supply method, catholyte, and applied potential. XRD and XPS were applied to investigate the status of Cu_xO catalyst and reaction interfaces, as shown in Fig. 4.

Cu_xO applied as the catalyst in this study is a mixture of Cu_2O (main), CuO and Cu as observed in its XRD pattern (Fig. 4a). The reduction of Cu_xO to Cu˚ has much less negative potential than eCO_2RR as found in the CV results in Figure S3. Thus, under the reaction potential of eCO_2RR, the Cu_xO catalyst should be reduced to Cu˚ rapidly. The XRD patterns of the two "after reaction" samples indicate the main component in the bulk catalyst after reaction either in 1.0 M $KHCO_3$ or 1.0 M KOH was metallic Cu. However, even though the bulk Cu_xO catalyst reduced to Cu˚, the catalytic activity maintained over 4 h with stable C_2 FE between 30–40%, as shown in Figure S6, suggesting the catalytic activity of Cu based catalyst may still be from Cu and OH or oxygen groups from oxide-derived catalyst could further reduce the activation energy and be favourable to carbonaceous products formation. XPS which was used to characterise the catalyst surface further proved this. Fig. 4b displays the XPS spectra on Cu_xO-GDE before eCO_2RR and after 3 h eCO_2RR in GDE cell with 1.0 M KOH and 1.0 M $KHCO_3$. The reduction of the catalyst after reaction is also observed since the satellite peaks of Cu $2p_{3/2}$ and Cu $2p_{2/1}$ on the fresh catalyst are both largely attenuated after reaction [51]. These peaks are stronger mitigated in the "after reaction ($KHCO_3$)" catalyst than those of "after reaction (KOH)", indicating the catalyst surface after reaction remains

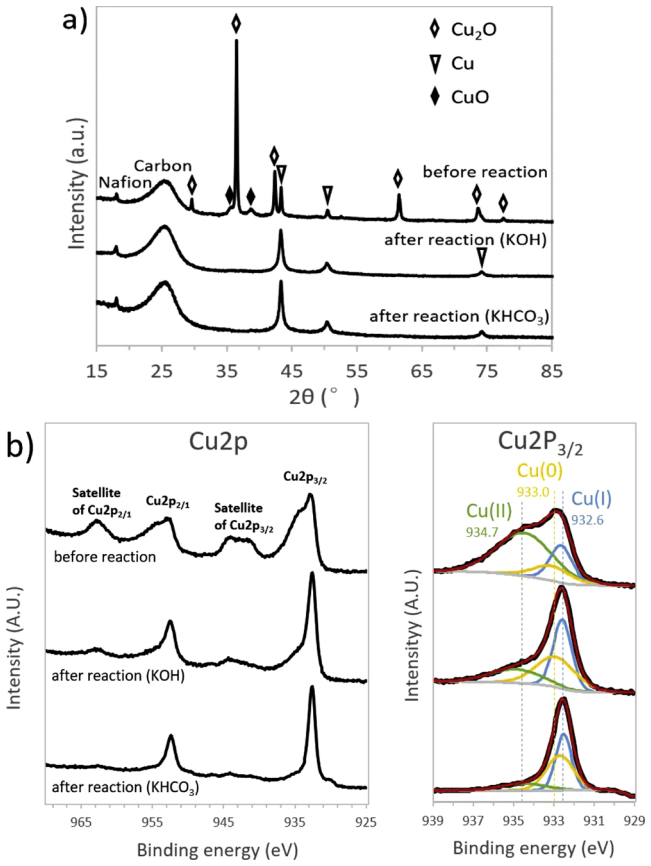

Fig. 4. a) XRD patterns and b) XPS spectra of Cu2P and the peak-differentiating of $Cu2P_{3/2}$ for the Cu_xO-GDE before eCO_2RR and after 3 h eCO_2RR in 1.0 M KOH and 1.0 M $KHCO_3$.

higher oxidation degree in KOH than in $KHCO_3$. The $Cu2P_{3/2}$ photoelectric peak was fitted to quantitatively analysis Cu species [52,53]. The fresh catalyst surface contains 14.65% Cu(0), 21.99% Cu(I), and 63.36% Cu(II). After eCO_2RR, the catalyst surface of "after reaction (KOH)" contains 37.82% Cu(0), 39.92% Cu(I) and 22.26% Cu(II), showing higher oxidation degree than that of "after reaction ($KHCO_3$)" containing 44.31% Cu(0), 41.15% Cu(I) and 14.54% Cu(II). Although the bulk Cu_xO catalyst was substantially reduced to metallic Cu after eCO_2RR, oxidized Cu partially remained on the catalyst surface.

In summary, the OH groups adsorbed on the catalyst surface may partially prevent the oxidised Cu surface from being reduced to metal and reduce the energy barrier of CO_2 activation through enhancing the adsorption strength [35] and stability of the active species CO* on reaction sites [3,36,37]. Also, the high concentration of OH^- on Cu catalyst surface showed reduced CO—CO coupling energy barrier [47], resulting in enhanced selectivity of C_2 products.

4. Conclusions

In this study, the effects of CO_2 supply method and alkalinity on the selectivity of carbonaceous products, and C_2 products were investigated in aqueous electrolyte using Cu_xO catalyst. The results suggested that GDE cell with CO_2 supplied through gas diffusion has higher selectivity for carbonaceous products and suppression of HER compared to two-chamber cell with CO_2 purging into electrolyte. Faradaic Efficiency of carbonaceous products increased from < 10% in 2C cell to 55% in GDE cell at -1.17 V in 1.0 M $KHCO_3$. This was primarily due to different reactants for CO_2 electrochemical reduction in GDE and in reaction solution, being CO_2* and hydrated H_2CO_3*, respectively. The alkalinity of catholyte also had a significant influence on the selectivity of

carbonaceous products leading to higher FE from KOH than $KHCO_3$. Higher FE of C_2 products, ethanol and ethylene, were observed from KOH with higher concentration (≥ 0.5 M) and at higher overpotentials (-0.97 and -1.17 V), suggesting C—C coupling process occurring with high concentration of OH at catalyst interface with high energy input. XRD and XPS proved the effect of OH groups on the catalysts surface could be favourable to carbonaceous products formation. At -1.17 V with 2 M KOH, C_2 FE achieved at 40% with current density -234 mA cm^{-2}, producing 0.105 mg min^{-1} ethylene and 0.035 mg min^{-1} ethanol on 2 cm^2 electrode with CO_2 flow rate 15 ml min^{-1}. This is promising for further development and scale-up.

Acknowledgement

The authors thank EPSRC LifesCO2R project (EP/N009746/1), EPSRC NECEM (EP/R021503/1) and NERC MeteoRR (NE/L014246/1). Hang Xiang thanks the Doctor Training Awards (SAgE DTA, 2015 cohort) from Faculty of Science, Agriculture and Engineering, Newcastle University for supporting PhD study. The authors are grateful to Ms Maggie White for XRD measurement, and Dr Isabel Garcia for SEM/EDX analysis. Data supporting this publication is openly available under an 'Open Data Commons Open Database License'. Additional metadata are available at: https://doi.org/10.17634/150659-4.

Appendix A. Supplementary data

Supplementary material related to this article can be found, in the online version, at doi:https://doi.org/10.1016/j.jcou.2019.02.007.

References

[1] B. Dáder, A. Fereres, A. Moreno, P. Trębicki, Elevated CO 2 impacts bell pepper growth with consequences to Myzus persicae life history, feeding behaviour and virus transmission ability, Sci. Rep. 6 (2016) 19120.
[2] B.P. Sullivan, K. Krist, H. Guard, Electrochemical and Electrocatalytic Reactions of Carbon Dioxide, Elsevier, 2012.
[3] D.D. Zhu, J.L. Liu, S.Z. Qiao, Recent advances in inorganic heterogeneous electrocatalysts for reduction of carbon dioxide, Adv. Mater. 28 (18) (2016) 3423–3452.
[4] A.J. Martín, G.O. Larrazábal, J. Pérez-Ramírez, Towards sustainable fuels and chemicals through the electrochemical reduction of CO 2: lessons from water electrolysis, Green Chem. 17 (12) (2015) 5114–5130.
[5] A.J. Bard, L.R. Faulkner, J. Leddy, C.G. Zoski, Electrochemical Methods: Fundamentals and Applications, wiley, New York, 1980, p. 2.
[6] J.K. Nørskov, T. Bligaard, A. Logadottir, J. Kitchin, J.G. Chen, S. Pandelov, U. Stimming, Trends in the exchange current for hydrogen evolution, J. Electrochem. Soc. 152 (3) (2005) J23–J26.
[7] Z.W. Seh, J. Kibsgaard, C.F. Dickens, I. Chorkendorff, J.K. Nørskov, T.F. Jaramillo, Combining theory and experiment in electrocatalysis: insights into materials design, Science 355 (6321) (2017) eaad4998.
[8] B. Endrődi, G. Bencsik, F. Darvas, R. Jones, K. Rajeshwar, C. Janáky, Continuous-flow electroreduction of carbon dioxide, Prog. Energy Combust. Sci. 62 (2017) 133–154.
[9] S. Rasul, A. Pugnant, E. Yu, Electrochemical reduction of CO2 at multi-metallic interfaces, ECS Trans. 85 (10) (2018) 57–66.
[10] K. Hara, A. Kudo, T. Sakata, Electrochemical reduction of carbon dioxide under high pressure on various electrodes in an aqueous electrolyte, J. Electroanal. Chem. Lausanne (Lausanne) 391 (1-2) (1995) 141–147.
[11] M. Todoroki, K. Hara, A. Kudo, T. Sakata, Electrochemical reduction of high pressure CO2 at Pb, Hg and in electrodes in an aqueous KHCO3 solution, J. Electroanal. Chem. Lausanne (Lausanne) 394 (1-2) (1995) 199–203.
[12] K. Hara, A. Tsuneto, A. Kudo, T. Sakata, Electrochemical reduction of CO 2 on a Cu electrode under high pressure factors that determine the product selectivity, J. Electrochem. Soc. 141 (8) (1994) 2097–2103.
[13] M. Azuma, K. Hashimoto, M. Hiramoto, M. Watanabe, T. Sakata, Electrochemical reduction of carbon dioxide on various metal electrodes in low-temperature aqueous KHCO 3 media, J. Electrochem. Soc. 137 (6) (1990) 1772–1778.
[14] S. Kaneco, H. Katsumata, T. Suzuki, K. Ohta, Electrochemical reduction of CO2 to methane at the Cu electrode in methanol with sodium supporting salts and its comparison with other alkaline salts, Energy Fuels 20 (1) (2006) 409–414.
[15] S. Ohya, S. Kaneco, H. Katsumata, T. Suzuki, K. Ohta, Electrochemical reduction of CO 2 in methanol with aid of CuO and Cu 2 O, Catal. Today 148 (3) (2009) 329–334.
[16] M. Alvarez-Guerra, J. Albo, E. Alvarez-Guerra, A. Irabien, Ionic liquids in the electrochemical valorisation of CO 2, Energy Environ. Sci. 8 (9) (2015) 2574–2599.
[17] S. Park, J.-W. Lee, B.N. Popov, A review of gas diffusion layer in PEM fuel cells: materials and designs, Int. J. Hydrogen Energy 37 (7) (2012) 5850–5865.
[18] D.-M. Feng, Y.-P. Zhu, P. Chen, T.-Y. Ma, Recent advances in transition-metal-Mediated electrocatalytic CO2 reduction: from homogeneous to heterogeneous systems, Catalysts 7 (12) (2017) 373.
[19] J. Wu, F.G. Risalvato, P.P. Sharma, P.J. Pellechia, F.-S. Ke, X.-D. Zhou, Electrochemical reduction of carbon dioxide II. Design, assembly, and performance of low temperature full electrochemical cells, J. Electrochem. Soc. 160 (9) (2013) F953–F957.
[20] H.R. Jhong, F.R. Brushett, P.J. Kenis, The effects of catalyst layer deposition methodology on electrode performance, Adv. Energy Mater. 3 (5) (2013) 589–599.
[21] M.R. Thorson, K.I. Siil, P.J. Kenis, Effect of cations on the electrochemical conversion of CO2 to CO, J. Electrochem. Soc. 160 (1) (2013) F69–F74.
[22] S. Ma, M. Sadakiyo, R. Luo, M. Heima, M. Yamauchi, P.J. Kenis, One-step electrosynthesis of ethylene and ethanol from CO 2 in an alkaline electrolyzer, J. Power Sources 301 (2016) 219–228.
[23] J. Wu, S. Ma, J. Sun, J.I. Gold, C. Tiwary, B. Kim, L. Zhu, N. Chopra, I.N. Odeh, R. Vajtai, A metal-free electrocatalyst for carbon dioxide reduction to multi-carbon hydrocarbons and oxygenates, Nat. Commun. (2016) 7.
[24] X. Lu, D.Y. Leung, H. Wang, J. Xuan, A high performance dual electrolyte microfluidic reactor for the utilization of CO 2, Appl. Energy 194 (2017) 549–559.
[25] J. Albo, A. Irabien, Cu2O-loaded gas diffusion electrodes for the continuous electrochemical reduction of CO2 to methanol, J. Catal. 343 (2016) 232–239.
[26] Z. Zhang, H. Che, J. Gao, Y. Wang, X. She, J. Sun, P. Gunawan, Z. Zhong, F. Su, Shape-controlled synthesis of Cu2O microparticles and their catalytic performances in the Rochow reaction, Catal. Sci. Technol. 2 (6) (2012) 1207–1212.
[27] Y. Hori, A. Murata, R. Takahashi, Formation of hydrocarbons in the electrochemical reduction of carbon dioxide at a copper electrode in aqueous solution, J. Chem. Soc., Faraday Trans. 1 85 (8) (1989) 2309–2326.
[28] B. Kumar, M. Llorente, J. Froehlich, T. Dang, A. Sathrum, C.P. Kubiak, Photochemical and photoelectrochemical reduction of CO2, Annu. Rev. Phys. Chem. 63 (2012) 541–569.
[29] H. Zhong, K. Fujii, Y. Nakano, F. Jin, Effect of CO2 bubbling into aqueous solutions used for electrochemical reduction of CO2 for energy conversion and storage, J. Phys. Chem. C 119 (1) (2014) 55–61.
[30] S. Zarghami, F. Boukadi, Y. Al-Wahaibi, Diffusion of carbon dioxide in formation water as a result of CO 2 enhanced oil recovery and CO 2 sequestration, J. Pet. Explor. Prod. Technol. 7 (1) (2017) 161–168.
[31] J. Resasco, L.D. Chen, E. Clark, C. Tsai, C. Hahn, T.F. Jaramillo, K. Chan, A.T. Bell, Promoter effects of alkali metal cations on the electrochemical reduction of carbon dioxide, J. Am. Chem. Soc. 139 (32) (2017) 11277–11287.
[32] J. Zhang, PEM fuel cell electrocatalysts and catalyst layers: fundamentals and applications, Springer Science & Business Media (2008).
[33] C.W. Li, M.W. Kanan, CO2 reduction at low overpotential on Cu electrodes resulting from the reduction of thick Cu2O films, J. Am. Chem. Soc. 134 (17) (2012) 7231–7234.
[34] Y.-J. Zhang, A.A. Peterson, Oxygen-induced changes to selectivity-determining steps in electrocatalytic CO 2 reduction, Phys. Chem. Chem. Phys. 17 (6) (2015) 4505–4515.
[35] C. Liu, M.P. Lourenço, S. Hedström, F. Cavalca, O. Diaz-Morales, H.A. Duarte, A. Nilsson, L.G. Pettersson, Stability and effects of subsurface oxygen in oxide-derived Cu catalyst for CO2 reduction, J. Phys. Chem. C 121 (45) (2017) 25010–25017.
[36] S. Rasul, D.H. Anjum, A. Jedidi, Y. Minenkov, L. Cavallo, K. Takanabe, A highly selective copper–indium bimetallic electrocatalyst for the electrochemical reduction of aqueous CO2 to CO, Angew. Chem. 127 (7) (2015) 2174–2178.
[37] D. Kim, S. Lee, J.D. Ocon, B. Jeong, J.K. Lee, J. Lee, Insights into an autonomously formed oxygen-evacuated Cu 2 O electrode for the selective production of C 2 H 4 from CO 2, Phys. Chem. Chem. Phys. 17 (2) (2015) 824–830.
[38] F. Calle-Vallejo, M. Koper, Theoretical considerations on the electroreduction of CO to C2 species on Cu (100) electrodes, Angew. Chem. 125 (28) (2013) 7423–7426.
[39] J.H. Montoya, C. Shi, K. Chan, J.K. Nørskov, Theoretical insights into a CO dimerization mechanism in CO2 electroreduction, J. Phys. Chem. Lett. 6 (11) (2015) 2032–2037.
[40] X. Nie, M.R. Esopi, M.J. Janik, A. Asthagiri, Selectivity of CO2 reduction on copper electrodes: the role of the kinetics of elementary steps, Angew. Chem., Int. Ed. 52 (9) (2013) 2459–2462.
[41] D.W. DeWulf, T. Jin, A.J. Bard, Electrochemical and surface studies of carbon dioxide reduction to methane and ethylene at copper electrodes in aqueous solutions, J. Electrochem. Soc. 136 (6) (1989) 1686–1691.
[42] K. Schouten, Y. Kwon, C. Van der Ham, Z. Qin, M. Koper, A new mechanism for the selectivity to C 1 and C 2 species in the electrochemical reduction of carbon dioxide on copper electrodes, Chem. Sci. 2 (10) (2011) 1902–1909.
[43] H. Xiao, T. Cheng, W.A. Goddard III, Atomistic mechanisms underlying selectivities in C1 and C2 products from electrochemical reduction of CO on Cu (111), J. Am. Chem. Soc. 139 (1) (2016) 130–136.
[44] D. Ren, Y. Deng, A.D. Handoko, C.S. Chen, S. Malkhandi, B.S. Yeo, Selective electrochemical reduction of carbon dioxide to ethylene and ethanol on copper (I) oxide catalysts, ACS Catal. 5 (5) (2015) 2814–2821.
[45] Y. Lum, J.W. Ager, Stability of residual oxides in oxide-derived copper catalysts for electrochemical CO2 reduction investigated with 18O labeling, Angew. Chemie Int. Ed. 57 (2) (2018) 551–554.
[46] H. Mistry, A.S. Varela, C.S. Bonifacio, I. Zegkinoglou, I. Sinev, Y.-W. Choi, K. Kisslinger, E.A. Stach, J.C. Yang, P. Strasser, Highly selective plasma-activated copper catalysts for carbon dioxide reduction to ethylene, Nat. Commun. 7 (2016) 12123.
[47] C.-T. Dinh, T. Burdyny, M.G. Kibria, A. Seifitokaldani, C.M. Gabardo, F.P.G. de Arquer, A. Kiani, J.P. Edwards, P. De Luna, O.S. Bushuyev, CO2 electroreduction to

ethylene via hydroxide-mediated copper catalysis at an abrupt interface, Science 360 (6390) (2018) 783–787.
[48] J. Albo, A. Sáez, J. Solla-Gullón, V. Montiel, A. Irabien, Production of methanol from CO2 electroreduction at Cu2O and Cu2O/ZnO-based electrodes in aqueous solution, Appl. Catal. B 176 (2015) 709–717.
[49] J. Albo, G. Beobide, P. Castaño, A. Irabien, Methanol electrosynthesis from CO2 at Cu2O/ZnO prompted by pyridine-based aqueous solutions, J. Co2 Util. 18 (2017) 164–172.
[50] J. Albo, D. Vallejo, G. Beobide, O. Castillo, P. Castaño, A. Irabien, Copper-based metal–Organic porous materials for CO2 electrocatalytic reduction to alcohols, ChemSusChem 10 (6) (2017) 1100–1109.
[51] F. Severino, J.L. Brito, J. Laine, J. Fierro, A.L. Agudo, Nature of copper active sites in the carbon monoxide oxidation on CuAl2O4and CuCr2O4Spinel type catalysts, J. Catal. 177 (1) (1998) 82–95.
[52] T.V.K. Karthik, M.d.l.L. Olvera, A. Maldonado, H. Gómez Pozos, CO Gas sensing properties of pure and Cu-incorporated SnO2 nanoparticles: a study of Cu-induced modifications, Sensors 16 (8) (2016) 1283.
[53] K.L. Deutsch, B.H. Shanks, Active species of copper chromite catalyst in C–O hydrogenolysis of 5-methylfurfuryl alcohol, J. Catal. 285 (1) (2012) 235–241.